Results in Chemistry 4 (2022) 100263

Contents lists available at ScienceDirect

Results in Chemistry

journal homepage: www.sciencedirect.com/journal/results-in-chemistry

2-Phenoxyacetamide derivatives as SARS-CoV-2 main protease inhibitor: In silico studies

Pandu Hariyono [a], Rini Dwiastuti [a], Muhammad Yusuf [b], Nurul H. Salin [c], Maywan Hariono [a,*]

[a] Faculty of Pharmacy, Sanata Dharma University, Campus 3, Paingan, Maguwoharjo, Depok, Sleman 55282, Yogyakarta, Indonesia
[b] Chemistry Department, Faculty of Mathematics and Natural Sciences, Padjadjaran University, Jatinangor, Sumedang 45363, West Java, Indonesia
[c] Malaysian Institute of Pharmaceuticals and Nutraceuticals, National Institute of Biotechnology Malaysia, Halaman Bukit Gambir, 11900 Bayan Lepas, Pulau Pinang, Malaysia

ARTICLE INFO

Keywords:
2-Phenoxyacetamide
SARS-CoV-2
Main protease
In silico

ABSTRACT

2-Phenoxyacetamide group has been identified as one of markers in the discovery and development of SARS-CoV-2 antiviral agent through its main protease (M^{pro}) inhibition pathway. This study aims to study a series of 2-phenoxyacetamide derivatives using *in silico* method toward SARS-CoV-2 M^{pro} as the protein target. The study was initiated by employing structure-based pharmacophore to virtually screen and to select the ligands, which have the best fit score (hits) along with the common pharmacophore features being matched. The result shows that from the 11 ligands designed, four ligands are selected as the hits by demonstrating fit score in the range of 56.20 to 65.53 to the pharmacophore model, employing hydrogen bond acceptor (HBA) and hydrophobic (H) as the common features. The hits were then docked into the binding site of the M^{pro} to see the binding mode of the corresponding hits as well as its affinity. The docking results free energy of binding (ΔG_{bind}) of the hits are in agreement with the pharmacophore fit score, in the range of −6.83 to −7.20 kcal/ mol. To gain the information of the hits as a potential drug to be developed, the *in silico* study was further proceed by predicting the mutagenic potency, toxicity and pharmacokinetic profiles. Based on the efficiency percentage, all hits meet the criteria as drug candidates by showing 84–88% leading to a conclusion that 2-phenoxyacetamide derivatives are beneficial to be marked as the lead compound for SARS-CoV-2 M^{pro} inhibitor.

Introduction

Regarding with COVID-19 pandemic, up to September 2021, WHO has been reporting 225,680,357 confirmed cases and 4,644,740 deaths since it was outbreak in early 2020 [1]. The spread chain of severe acute respiratory syndrome coronavirus 2 (SARS-CoV-2) is rapidly circulated inter-human through mouth droplets and also suspectedly by airborne, while no specific antiviral drug has been found to combat the viral replication [2]. On the other hand, although vaccination has reached about 40% of the world population, however to date, the herd immunity seems like still a long way to go, especially to the third-fourth world countries [3]. The repurposed drug such as hydroxy-chloroquine, oseltamivir, lopinavir and ivermectin could be lifesaving, however, it is not applicable in some cases having the drug contraindications [4]. Therefore, a specific drug is indispensable to minimize adverse drug reaction as well as to maximize the drug effectiveness.

To tail with the drug specificity, the finding of a new drug has been well-known to do by identifying the molecular targets at the initial step in which protein/ enzyme is one of the targets [5,6]. SARS-CoV-2 is composed by structural proteins (spike, membrane, envelope, capsid, ssRNA) and the non-structural proteins (nsp1-nsp16) with their integrated function to maintain the virus life cycle [7]. Main protease (M^{pro}) is the nsp5 having a function in the polypeptide1a and polypeptide1ab proteolysis to yield various small protein fragments to further be constructed and packed in new virions [8]. Therefore, by inhibiting this enzyme, the new virion formation would be canceled leading to a stopped viral replication [9].

During this one year, although it is still less, a series or individual peptidomimetic as well as small organic compounds have been evaluated for their inhibition against SARS-CoV-2 M^{pro} [10]. Initial study by Stoermer had been done by designing peptidomimetic inhibitor of SARS-CoV-2 M^{pro} through homology modeling raises an idea of utilizing peptide-based compound as this enzyme inhibitor [11]. Further study by Jin et al., had co-crystallized compounds *N*-[(5-methylisoxazol-3-yl)

* Corresponding author.
E-mail address: mhariono@usd.ac.id (M. Hariono).

https://doi.org/10.1016/j.rechem.2021.100263
Received 29 September 2021; Accepted 8 December 2021
Available online 12 December 2021

carbonyl]alanyl-l-valyl-*N* ~ 1~-((1*R*,2*Z*)-4-(benzyloxy)-4-oxo-1-{[(3*R*)-2-oxopyrrolidin-3-yl]methyl}but-2-enyl)-l-leucinamide or briefly named as N_3 as a potential SARS-CoV-2 M^{pro}, gave an immense value in the drug design of COVID-19 antiviral agent [12]. N_3 is a Michael acceptor peptidomimetic compound, mimicking lopinavir suggested to bind to the M^{pro} active site by interacting with the amino acid residues surround the sub-site 1′, 1, 2, and 4 (See Fig. 1). The subsite 1 (S1) is surrounded by PRO166, GLU189, THR190, and ALA191, while subsite 2 (S2) is flanked by the catalytic residue HIS41 and CYS145. Subsite 4 (S4) is indicated by SER46, whereas the subsite 1′ (S1′) is circumscribed by LEU141, ASN142, and GLU166. The most common interactions are hydrogen bond with GLU166, CYS145 and HIS163, supported by an extra-large hydrophobic interaction [13]. However, the character of peptidomimetic, which has a high flexibility, could cause its instability during pharmacokinetic steps as well as its pharmacodynamic behavior [14,15]. Therefore, a structural modification could be one of alternatives to improve the drug-like structure properties of this interesting ligand.

Interestingly, lopinavir is the protease inhibitor of Human Immunodeficiency Virus (HIV) currently repurposed for the treatment of COVID-19 patient [16]. This HIV antiviral agent bears 2-phenoxyacetamide group, which is similar to the benzyl acetyl group in N_3, has been identified as one of the important parts in binding the protease (see Fig. 2). This scaffold is feasible to be either synthesized or simply purchased from the supplier (Sigma Aldrich) [17–19].

In this present study, we investigate a series of 2-phenoxyacetamide derivatives using *in silico* methods toward SARS-CoV-2 M^{pro} as the protein target. The *in silico* study was initiated by employing structure-based pharmacophore to virtually screen and to select the ligands, which have the best fit score (hits) along with its common pharmacophore features. To avoid the hits potentially to be pan-assay interference compounds (PAINS) compounds, the online filter was conducted. The hits were then docked into the binding pocket of the M^{pro}, to see the binding mode of the corresponding hits as well as its affinity. To gain the information of the hits as a potential drug to be developed, the *in silico* study was further proceed by predicting their mutagenic potency, toxicity and pharmacokinetic profiles.

Materials and method

Hardware and software

A laptop with the following specifications: AMD Ryzen 3 2200U, VGA Radeon Vega 3, RAM 4 GB and HDD 1 TB. The 3D protein structure of SARS-CoV-2 M^{pro} was collected from protein data bank (PDB 6M2N). Other softwares were Marvin Sketch (www.chemaxon.com), AutoDockTools1.5.6 package (www.autodock.scripps.edu), false positive remover online tool (https://www.cbligand.org/PAINS/), LigandScout4.4.7 (www.inteligand.com), pKCSM online tool (http://biosig.unimelb.edu.au/pkcsm/prediction) and Biovia Discovery Studio 2021 (www.accelrys.com).

Structure-based pharmacophore mapping

The structure-based pharmacophore mapping used the pharmacophore model of baicalein bound to SARS-CoV-2 M^{pro} (PDB 6M2N) [20], which had been generated and validated in our previous study [21]. The ligands were sketched using Marvin Sketch and converted into 3D structure using Biovia Discovery Studio. The ligand was protonated when it had a basic amine group, whereas it was deprotonated, when it had an acidic carboxylate group. The ligands were then screened into the individual pharmacophore using screening tool with the parameters as follow: scoring functions = pharmacophore-fit; max numbers of omitted features = 2; compounds time out = 0 min; screening mode: match all query features; retrieval mode = stop after first matching conformation; and execution mode = multi-threaded.

Molecular docking study

The crystal structures of SARS-CoV-2 M^{pro} with their co-crystallized ligands i.e., 5,6,7-trihydroxy-2-phenyl-4H-chromen-4-one (baicalein; PDB 6M2N) was downloaded from the Protein Data Bank (PDB) (www.rcsb.org). The HIS41 at the catalytic site was protonated at N_π. The docking protocol refers to our previous publication [21], which is briefly prepared as following: The grid box was 40, 40, 40 in size with 0.375 Å space and centre x = −9.732, y = 11.403, z = 68.925. The docking was run 250 times using AutoDock4.2 with the default parameters as

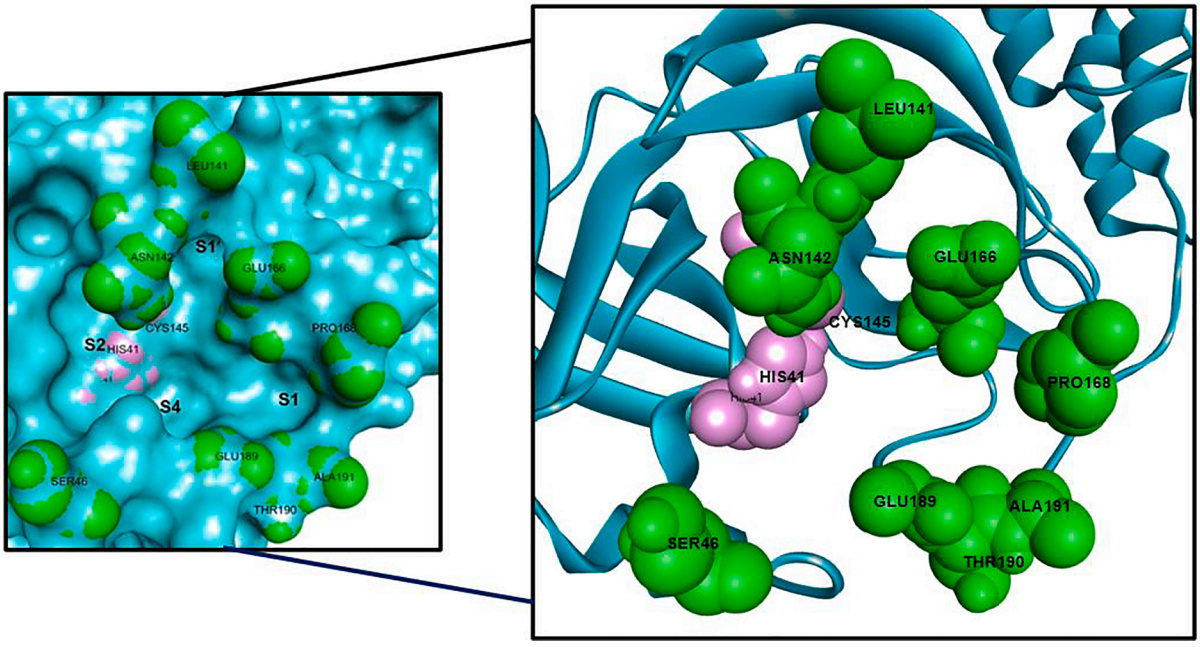

Fig. 1. The surface binding pocket of SARS-CoV-2 M^{pro} with four subsites (S1′, S1, S2 and S4) with their surrounding residues. The pink area is the catalytic dyad, whereas the green areas are the residues that flank the catalytic cavity. Inset is the solid ribbon in combined with CPK model of the M^{pro} protein.

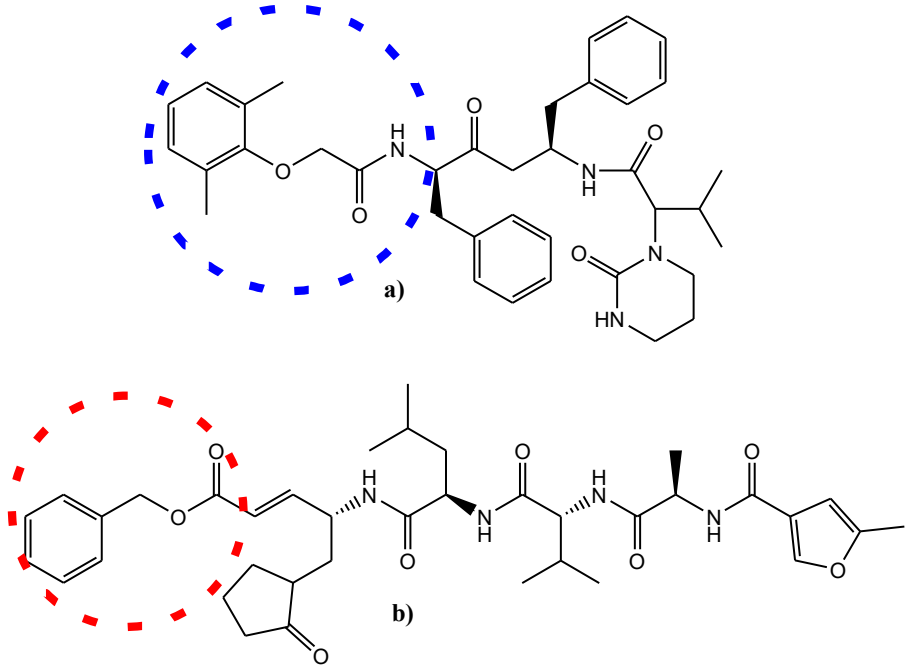

Fig. 2. The structure of a) lopinavir and b) N_3 with the blue dashed circle is 2-phenoxyacetamide group, whereas the red dashed circle is benzyl acetyl, which mimics to 2-phenoxyacetamide group.

followed: population size = 150, number of evaluations = 2,500,000, number of generations = 27,000, elitism = 1, mutation rate = 0.02, crossover rate = 0.8, and rmstol = 2 [22].

PAINS filter

The PAINS filter was carried out by inputting the SMILES string in the searching machine (https://www.cbligand.org/PAINS/). The prediction was done by clicking the searching machine and the result was obtained by showing whether it passed the PAINS filter [23].

Drug-like structure

The drug-like structure profile were individually predicted by inputting its SMILES string, which is automatically done by the server. The value of molecular weight (MW), partition coefficient (log P), the number of hydrogen bond donors (HBD), the number of hydrogen bond acceptors (HBA), the number of rotatable bonds and the surface area, were observed and then tabulated [24].

Mutagenic potency and toxicity studies

Using the same protocol in Section 2.5, the mutagenic potency of the ligands was represented by the AMES test result. Instead, other parameters such as maximum tolerated dose (human) (hMTD), human Ether-à-go-go-Related Gene (hERG) I inhibitor, hERG II inhibitor, oral rat acute toxicity (log LD_{50}), oral rat chronic toxicity (log LOAEL), hepatotoxicity, skin sensitization, *T. pyriformis* toxicity, and minnow toxicity represented the toxicity properties of the ligands [24].

Pharmacokinetics study

Using the same protocol in 2.5, the ADME (absorption, distribution, metabolism, and excretion) profiles of the ligands were predicted. Subsequently, the absorption is influenced by water solubility, Caco2 permeability, skin permeability, P-glycoprotein substrate, P-glycoprotein I inhibitor, and P-glycoprotein II inhibitor, instead of human gastrointestinal absorption. The distribution is represented by VDss (human), fraction unbound (human), blood–brain barrier (BBB) permeability, and central nervous system (CNS) permeability. The metabolism is represented by the CYP2D6 substrate, CYP3A4 substrate, CYP1A2 inhibitor, CYP2C19 inhibitor, CYP2C9 inhibitor, CYP2D6 inhibitor, and CYP3A4 inhibitor. Lastly, the excretion is represented by total clearance and renal OCT2 substrate. The drug-like structure, mutagenic potency, toxicity and pharmacokinetic predictions were carried using pkCSM online tool (http://biosig.unimelb.edu.au/pkcsm/prediction) [24].

Results

As previously published, the pharmacophore model has a pentagon shape which is composed by three hydrogen bond acceptor (HBA) features and two hydrophobic (H) features with various inter-distances as followed: H-H (6.15 Å), H-HBA (2.38 Å), HBA-HBA (2.76 Å), HBA-HNA (5.14 Å), and HBA-H (6.93 Å). Eleven ligands have been screened against the pharmacophore model (see Fig. 1a) and showing 10 ligands having similar fit score i.e., in range of 55.47 to 56.20 (see Table 1). The common features of those 10 ligands are same employing four HBA and one H. The best fit score goes to Ligand **6** (65.53) which has an extra H as the common feature. This result reflects that all 2-phenoxyacetamide derivatives have a potential to have a binding mode mimicking

Table 1
The screening results of ligand **1**–**11** against baicalein pharmacophore model.

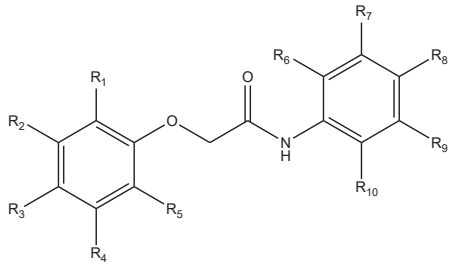

Ligands	R_1	R_2	R_3	R_4	R_5	R_6	R_7	R_8	R_9	R_{10}	Fit-score	Common Features
1	H	H	H	H	H	H	H	H	H	Cl	56.20	4HBA, 1H
2	H	H	H	H	H	H	H	H	H	OH	57.00	4HBA, 1H
3	H	H	H	H	H	H	H	H	H	COOH	56.20	4HBA, 1H
4	H	H	H	H	H	H	H	H	COOH	H	55.71	4HBA, 1H
5	H	H	H	H	H	H	H	H	$COCH_3$	H	55.68	4HBA, 1H
6	H	H	H	H	H	H	H	$COCH_3$	H	H	65.53	4HBA, 2H
7	H	H	H	H	H	H	H	NO_2	H	H	55.47	4HBA, 1H
8	H	H	H	H	H	H	C_6H_5	OH	C_6H_5	H	55.87	4HBA, 1H
9	H	H	CH_3	H	H	H	H	H	OH	H	55.86	4HBA, 1H
10	H	H	H	H	H	C_2H_4OH					55.88	4HBA, 1H
11	H	H	H	H	H	naphthyl					55.86	4HBA, 1H

baicalein as the reference of SARS-CoV-2 M^{pro} inhibitor. However, we are interested to those who have fit score greater than 55. They are ligand **1**, **2**, **3** and **6** varied by *o*-Cl, *o*-OH, *o*-COOH and *p*-$COCH_3$, respectively toward the amide group.

Ligand **6** has the best fit score, which is contributed by O-acetyl and O-amide as the HBA, whereas the H features are contributed by two phenyl rings (see Fig. 3b). The second-best ligand goes to ligand **2**, in which the fit score is contributed by O-Phenolic and O-amide as the HBA, and again, one phenyl ring linked to amide has a contribution to the H feature (see Fig. 3c). Two ligands (**1** and **3**) have a same fit score, however, the HBAs are contributed by slightly different functional groups (see Fig. 3d and 3e). In ligand **1**, HBAs are contributed by O-amide and O-ether, whereas in ligand **3**, it is contributed by O-amide and O-carboxylate, both in the carbonyl group as well as in the hydroxyl group. Commonly, the H features are contributed by phenyl ring, however, there is a different phenyl ring contributing as H features in ligand **1** and **3**. The H feature in ligand **1** is contributed by phenyl linked to the ether bridge, whereas in ligand **3**, it is linked to the amide group.

Docking study shows an order of agreement between free energy of binding (ΔG_{bind}) and the fit score from the pharmacophore mapping. The overlapping pose of the hits is presented in a surface protein model, showing their similar occupation in the main pocket of SARS-CoV-2 M^{pro} (see Fig. 4). However, the sub-pocket (S) occupation is varied for all hits. Ligand **1** and **6** share a similar sub-pocket occupation at the arylamide phenyl ring (sub-pocket 4 (S4)), whereas the phenoxy phenyl rings are oriented to S1′ and S1 for ligand **1** and ligand **6**, respectively. In contrast, the S4 is shared by the phenoxy phenyl ring of Ligand **2** dan **3**, whereas the arylamide phenyl rings are oriented to the S1′ and S1 for ligand **3** and ligand **2**, respectively. Overall, according to the phenyl ring occupations, the pose of ligand **2** and ligand **6** is similar (oriented to the S4 and S1) instead of the type of phenyl ring is different. The same behavior is also occurred in ligand **1** dan ligand **3**, wherein the S4 and S1′ are occupied by phenyl ring with a different type of linker.

The lowest ΔG_{bind} (−7.20 kcal/ mol; see Table 2) goes to ligand **6**, which is contributed by Hydrogen Bond (H-Bond) interactions between O-amide with GLU166 and O-acetyl with GLY143, SER144, and CYS145. An attention could be drawn from the H-Bond with GLU166 due to its close distance measured in 2.12 Å and the catalytic residue CYS145 having H-bond distance in 2.15 Å. These H-bonds are then mainly supported by van der Waals (vdW) interactions with TYR54, PHE140, LEU141, ASN142, ASP187, ARG188, GLN189, and MET165. Further minor non-bonding interactions are as following: Pi-Pi stacked with HIS41, and Pi – Alkyl with MET49. Thus, all these binding modes may contribute to the lowest estimated K_i, 6.98 μM, which is defined as the minimum concentration of ligand **6** to competitively inhibit SARS-CoV-2 M^{pro} enzymatic activity.

Other docking profiles can be seen in Table 2, whereas the non-bonding interactions for Ligand **1**, **2**, and **3** can be seen in Table 3. An exception is observed in ligand **1**, in which no H-bond interaction occurs in this ligand's pose. The **o**-Cl group toward amide link seems like taking the HBA and HBD atoms in the linker of phenyl rings away from the surrounding HBD and HBA residues, leading to the absence of such H-Bond interaction. Therefore, the ΔG_{bind} is mainly contributed by vdW with ASP48, PRO52, TYR54, THR190, ALA191, LEU167, GLN192, ARG188, ASP187, and ASP187, followed by C–H bond with GLN189, Pi-Sulfur with CYS44 and Met165, Pi-Pi stacked with HIS44, Pi-Alkyl with MET49 and PRO168 (see Fig. 5).

Working with enzymatic system, a false-positive result often raises due to some factors. These are covalent modifications, redox effects, chelation, autofluorescence, or degradation, which could be a signal of the false-positive results under *in vitro* assay condition, which is then called as pan-assay interference compounds (PAINS) [25]. Here, the hits were filtered to predict whether they have a potential PAINS property, thus, they should be put beside from the next process. The result shows that no hit is predicted to have this PAINS property, therefore, all hits pass to the next step of the drug-like structure characterization.

Lipinski Rule limits an ideal drug-like structure should have<500 Da in molecular weight (MW), partition coefficient (log P) < 5, the number

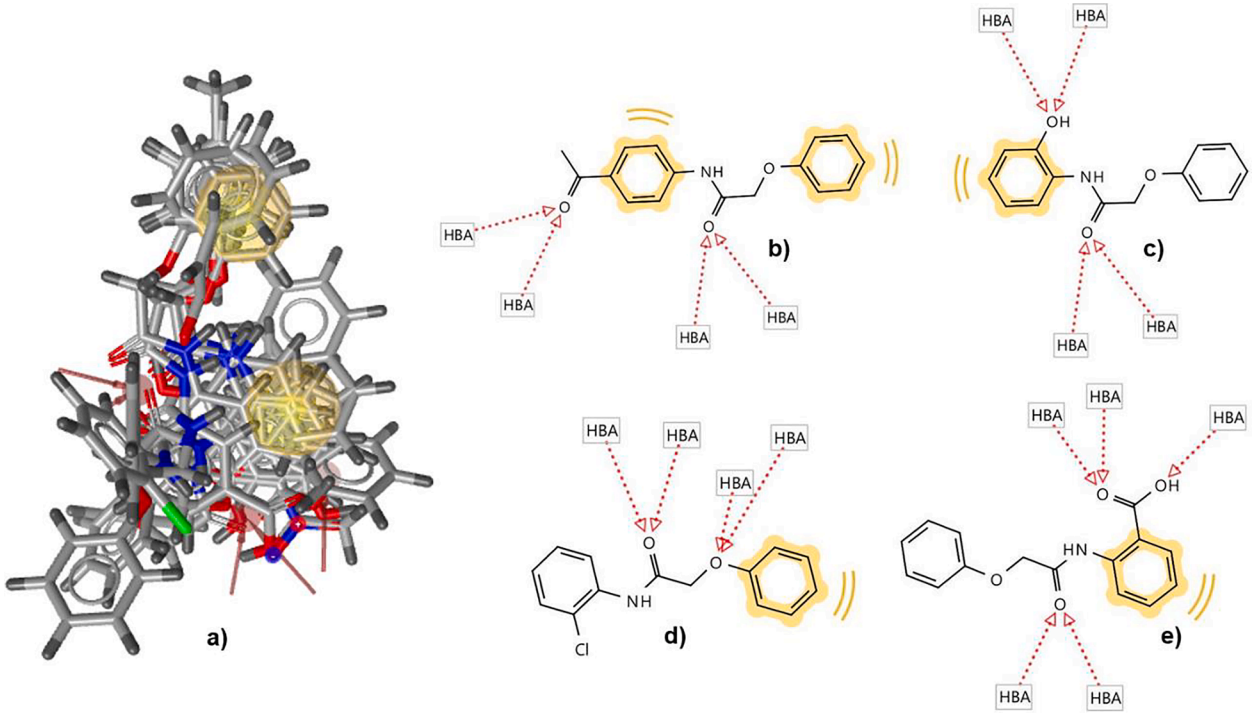

Fig. 3. The structures of a) overlapping 3D ligand **1**–**11** and the 2D structure of b) ligand **6**, c) ligand **2**, d) ligand **1** and e) ligand **3**, map to the baicalein pharmacophore model. Red dashed arrow and yellow ring represent HBA and H, respectively.

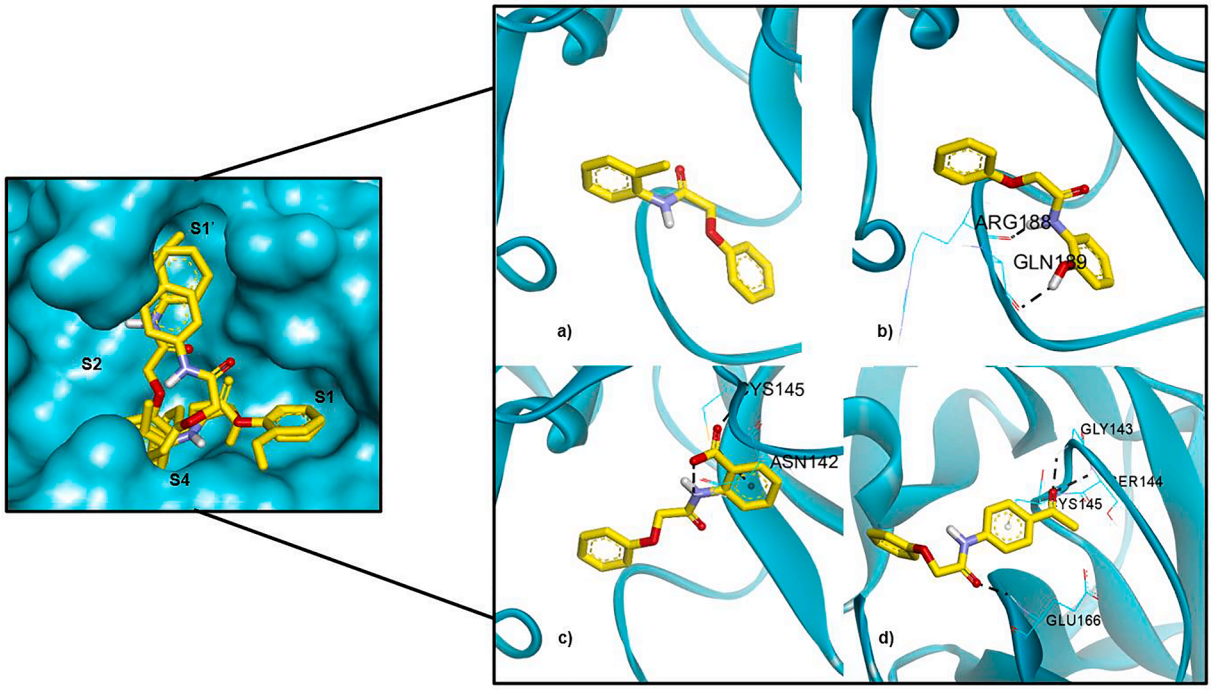

Fig. 4. The overlapping poses of the hits in the binding pocket of SARS-CoV-2 M^{pro} (surface model). Inset is the individual docking poses of a) ligand 1, b) ligand 2, c) ligand 3, and d) ligand 6 in the ribbon model. The black dashed lines represent the H-Bond interactions.

Table 2
The docking results of the hits against SARS-CoV-2 Mpro.

Ligand	ΔG_{bind} (kcal/mol)	H-Bond Interacting Residue (Distance (Å))	Estimated K_i (μM)
1	−6.84	–	9.62
2	−6.74	ARG188 (2.00), GLN189 (2.05)	11.40
3	−6.83	ASN142 (2.37), CYS145 (1.80; 3.16)	9.81
6	−7.03	GLY143 (2.19), SER144 (2.44), CYS145 (2.15), GLU166 (2.12)	6.98
Baicalein	−6.38	GLY143 (2.96), GLU166 (3.11)	9.64

Table 3
The non-bonding interactions of the hits with SARS-CoV-2 M^{pro} binding pocket.

Ligands	van der Waals	C–H bond	Pi-Sulfur	Pi-Pi Stacked	Pi-Alkyl
1	ASP48, PRO52, TYR54, THR190, ALA191, LEU167, GLN192, ARG188, ASP187, ASP187	GLN189	CYS44, MET165	HIS41	MET49, PRO168
2	ASP48, PRO52, TYR54, GLU166, THR190, ALA191, LEU167, GLN192, ASP187	–	CYS44, MET165	HIS41	MET49, PRO168, THR190
3	PRO52, TYR54, ARG188, ASP187, GLN189, HIS164, MET165, GLU166, PHE140, LEU141, SER144	–	CYS44	HIS41	MET49
6	, TYR54, PHE140, LEU141, ASN142, ASP187, ARG188, GLN189, MET165,		5	HIS41	MET49

of hydrogen bond donor (HBD) ≤ 5, the number of hydrogen bond acceptor (HBA) ≤ 10, rotatable bonds ≤ 10, and surface area ≤ 140 Å [26,27]. In general, the result shows that all ligands passed the MW, the number of HBD, HBA rotatable bonds, and surface area limitations. Table 4 presents the chalcones with their Lipinski Rule profiles.

In general, a chemical's mutagenic properties are usually evaluated using the AMES test [28,29]. Furthermore, the toxicity to human can be measured using human maximum tolerated dose (hMTD), human Ether-à-go-go-Related Gene (hERG) effect, oral rat acute toxicity (log LD_{50}), oral rat chronic toxicity (log LOAEL), hepatotoxicity, skin sensitization, *T. pyriformis* toxicity, and minnow toxicity [30–32]. This hMTD is accepted when the estimated toxic dose threshold in humans is greater than 0.477. hERG I and II represent the potassium channels that mediate the cardiac repolarization in humans. Thus, inhibiting these genes would cause a long QT syndrome development that might lead to a fatal arrhythmia. The *in vivo* toxicity is frequently expressed by LD_{50} value, which can be defined as the lowest dose given to cause 50% death of a group of animals in testing a compound acute toxicity, represented by ORAT (log LD_{50} value) prediction. The safety of drugs to the environment is nowadays a concern. Low environmental damage is demonstrated by the values of *T. pyriformis* and minnow toxicity to be respectively higher than 0.5 and −0.3.

The AMES test indicates that no ligand shows mutagenic effect. Most of the hits have a low maximum dose which is weakly tolerated in humans, except for ligand **3**. No hits inhibit the both hERG, except for ligand **6**, which inhibits hERG II. Interestingly, all hits exhibit no skin sensitization as well as their hepatotoxicity. The oral rat acute toxicity LD_{50} can be grouped as very toxic (≤5mg/kg), toxic or moderately toxic (greater than5 to < 500 mg/kg), harmful or slightly toxic (greater than500 to < 2000 mg/kg), and non-toxic (greater than2000 mg/kg) [29]. After converting the log ORAT into its antilog, the ORAT value of ligand **1**, **2**, **3** and **6** are 132, 101, 34 and 478 mg/ kg, respectively. Therefore, ligand **3** show a potential toxic property, whereas ligand **1**, **2** and **6** show a potential moderate toxicity. In the chronic toxicities (ORCT), all hits could be categorized as a potential toxic to moderate toxic category. Except for ligand **3**, all hits do not demonstrate *T. pyriformis* toxicity potency, whereas, ligand **2** and ligand **3** show minnow

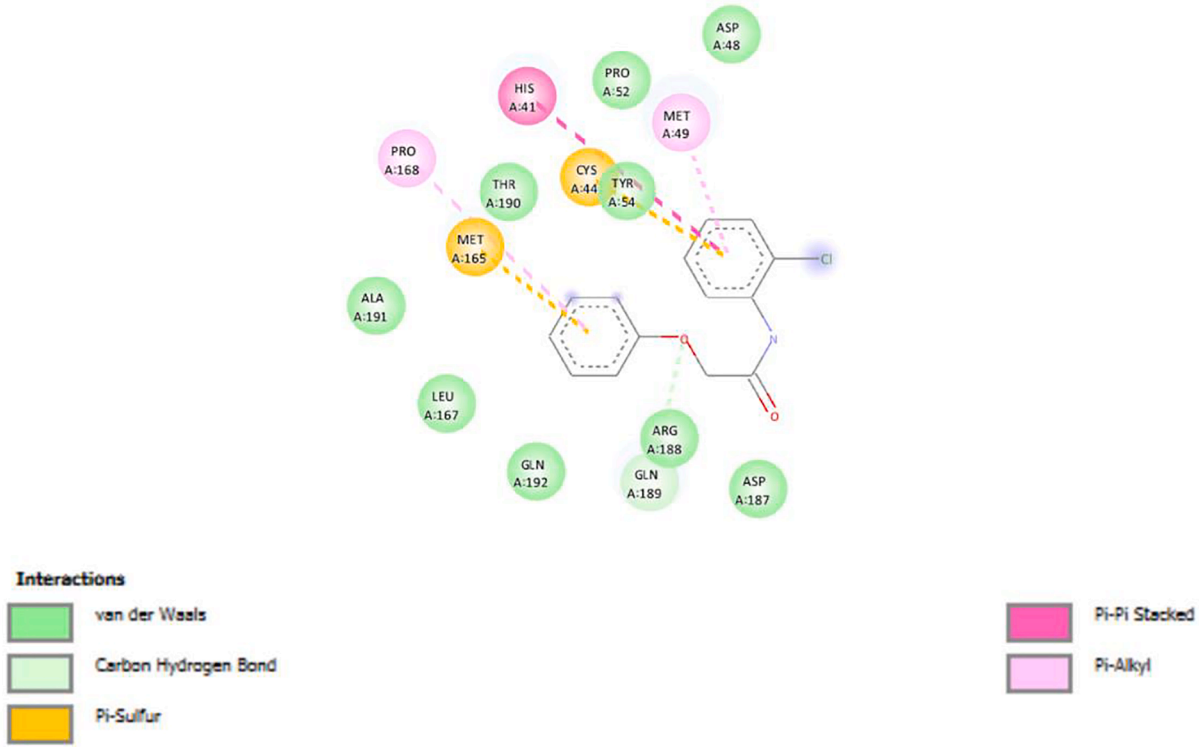

Fig. 5. The 2D diagram of ligand 1 pose in the binding pocket of SARS-CoV-2 M^{pro} possessing non-bonding interactions with surrounding residues.

Table 4
The drug-like structure evaluation results of the hits.

Ligands	MW	log P	HBD	HBA	Rotatable Bonds	Surface area
1	261.078	3.3575	4	2	1	110.347
2	243.262	2.4097	4	3	2	104.838
3	270.264	1.0676	5	4	1	115.364
6	269.300	2.9067	5	3	1	116.935

toxicity. Table 5 presents the AMES test result of the hits for mutagenicity prediction along with other toxicity profiles.

Table 6 demonstrates that almost all hits are well absorbed through the human intestine with nearer values to 100% into the blood system, except for ligand **3**, which only shows 58.026% human intestinal absorption. The water solubility of all hits in general are most likely accepted as their log S value are higher than −4, indicating that it may dissolve readily during the dissolution step. Furthermore, the Caco2 cell model for oral absorption prediction requires value greater than 0.90 [33]. Therefore, except ligand **3**, all hits show good human gastrointestinal absorption. The skin permeability of all hits is most likely suitable for the transdermal route because the values are approximately −2.5. A protein transport namely P-glycoprotein (P-gp) is vital during the pharmacokinetics steps, although this could have either benefited and unbenefited therapeutic effect [34]. A drug is supposed to not inhibit P-gp, either P-gp I or P-gp II and in the normal situation, it should not be acting as P-gp substrate either. According to the prediction, ligand **2** is predicted to act the P-gp substrate, whereas no hits inhibit both P-gp I and P-gp II.

Volume of distribution at steady state (VDss) is a parameter in distribution directly proportional with the amount of drug distributed into tissue; the more VD indicates the more amount of tissue distribution, which should be ≥ -0.15. Among the hits, there only ligand **3** do not meet these criteria. The fraction unbound (fu) for all hits are predicted to be < 0.15 except for ligand **2**, indicated that there is an interference from the plasma protein on the way of drug to the receptor. The drug distribution is also parameterized for their ability to cross the brain membrane which is important as the compounds may affect the central nervous system (CNS) [35]. The blood–brain barrier (BBB) and CNS permeability are poor when the value < -1 and < -3, respectively. This means that the compound is poorly distributed to the brain and unable to penetrate CNS. From the results, all hits should be carefully managed as there is potential to enter the CNS especially for ligand **1**, which can also penetrate BBB. Table 7 presented the distribution profiles of the hits as predicted by software.

Biotransformation or metabolisms are also important to indicate good drug-like properties. Subfamilies of cytochrome P450 namely CYP1A2, CYP2C9, CYP2C19, CYP2D6, and CYP3A4 have been studied playing essential roles in drug biotransformation [36]. Brain and

Table 5
The mutagenic potency and toxicity evaluation result of the hits.

Ligands	AMES toxicity	hMTD	hERG I inhibitor	hERG II inhibitor	ORAT (log LD_{50})	ORCT (log LOAEL)	Hepatotoxicity	Skin Sensitisation	*TP* toxicity	Minnow toxicity
1	No	0.396	No	No	2.412	2.016	No	No	1.569	-0.38
2	No	0.250	No	No	2.005	2.149	No	No	0.678	0.532
3	No	0.666	No	No	1.536	1.468	No	No	0.285	0.125
6	No	0.263	No	Yes	2.368	2.035	No	No	1.432	-0.524

*The red color indicates that the ligand does not meet the criteria of the corresponding parameter

Table 6
The absorption profile evaluation results of the hits.

Ligands	Water solubility	Caco2 permeability	Intestinal absorption (human)	Skin Permeability	P-glycoprotein substrate	P-glycoprotein I inhibitor	P-glycoprotein II inhibitor
1	-3.570	1.595	92.292	-2.682	No	No	No
2	-2.734	1.287	92.638	-2.760	Yes	No	No
3	-2.864	0.533	58.026	-2.375	No	No	No
6	-3.224	1.347	93.036	-2.752	No	No	No

*The red color indicates that the ligand does not meet the criteria of the corresponding parameter

intestines are the most organ, wherein respectively CYP2D6 and CYP3A4 are deposited. They most likely responsible to metabolize the drug in their surrounding areas. Furthermore, when a drug has first-pass metabolism, CYP3A4 is the main metabolizer. In this prediction, neither hits act as the substrate nor inhibitor for CYP2D6. However, ligand **1** and **6** act as CYP3A4 substrates and CYP2C19 inhibitors. Furthermore, except for ligand **3**, all hits are likely to inhibit CYP1A2, which should be of concern, when the compound is consumed with other drugs. Interestingly, no hit acts as inhibitor for CYP2C9 and CYP3A4 as presented in Table 8.

Upon metabolism, a drug is removed from the body, which can be indicated from its total clearance associated with the drug elimination rate [37]. On the other hand, OCT2 transporter works by renal up taking the drug from the blood. Most likely, the drug having cationic characters as well as endogenous compound will be prioritized to be removed and cleared from the body [38]. Cimetidine, H2 antagonist, had been studied to inhibit OCT2, thus, it elevates OCT2-dependent renal clearance drugs, which alters the pharmacokinetics and pharmacodynamics profiles. Ligand **3** is predicted to be the fastest compound excreted from the body due to its highest total clearance. In contrast, ligand **2** is the slowest compound to be removed from the body due to its lowest total clearance. However, all hits have low total clearance (log Cl $<$ 0.763), yet, it is generally desirable to develop a drug for oral administration without a high dosage regimen [39]. Interestingly, there is no ligand predicted to act as renal OCT2 substrate, that might be less to undesirable side effects. Table 9 presents the total clearance of all hits that reflects their speed to be eliminated from the body system.

Discussion

Structural modification of an existing compound has been applied since long time ago with various reasons [40]. These could be either enhancing the drug activity or reducing the toxicity. Other reasons could be improving the drug pharmacokinetic profiles or its physical–chemical stability. The chemical structure could be simplified to reduce the cost and time being consumed in the drug synthesis or production. However, this simplification should not extremely change the drug activity, thus, *in silico* study could be a good starting point to design a drug, which is feasible to be synthesized, while maintaining its pharmacophore features.

In this study, a series of 2-phenoxyacetamide derivatives has been designed as SARS-CoV-2 M^{pro} inhibitor by considering its synthetic feasibility as well as the pharmacophore features as generated from baicalein, a SARS-CoV-2 M^{pro} inhibitor. 2-phenoxyacetamide could be simply synthesized under acetylation between 2-phenoxyacetyl chloride and aromatic amine [41] or under alkylation of phenol using bromopropionyl chloride [42]. There are 11 2-phenoxyacetamide derivatives designed with mostly having modification at the arylamide phenyl ring. These modifications are carried out by attaching electron withdrawing groups (EWGs) such as Cl, COOH, NO_2 and phenyl in different positions [43]. On the other hand, some electron donating groups (EDGs) such as OH, C_2H_4OH and methyl are also implemented [43]. A combination between EWG and EDG, i.e. $COCH_3$ is also applied. Interestingly, all 11 ligands performed a considerably fit score toward the pharmacophore model with almost no significant difference, except for ligand **1**, **2**, **3** and **6**. The common pharmacophore features are also consistent for all ligands covering 4HBA and 1H features, except for ligand **6** with an extra 1H feature. However, the selected hits are most likely having EWG character than the EDG. Interestingly, the highest fit score goes to the ligand having a combination between EWG and EDG modification at the *para* position of the arylamide phenyl ring. This group is able to locate the position of both phenyl rings (arylamide and phenoxy) fit to the hydrophobic features, while other hits are only able to fit one hydrophobic feature. Thereby, it increases the fit score. This $COCH_3$ is also able to maintain the fitting with HBA features as others done.

The docking poses are dealt with the pharmacophore results. The phenyl rings could be a head and tail to nicely sit in the hydrophobic sub-pockets, while either the HBA or HBD interacts with the surrounding residues via H-Bond interactions. A more attention is drawn for ligand **6**, in which the $COCH_3$ at the *para* position could locate the NH-amide to interact with SER144 at a considerably close distance (2.44 Å). This phenomenon reminds us to the chymotrypsin protease character, in

Table 7
The distribution profile evaluation results of the hits.

Ligands	VDss (human)	Fraction unbound (fu) (human)	BBB permeability	CNS permeability
1	0.081	0.081	0.288	-0.96
2	0.11	0.167	-0.090	-2.261
3	-2.503	0.133	-0.165	-2.649
6	-0.096	0.071	-0.020	-2.203

*The red color indicates that the ligand does not meet the criteria of the corresponding parameter

Table 8
The metabolism profile evaluation results of the hits.

Ligands	CYP2D6 substrate	CYP3A4 substrate	CYP1A2 inhibitor	CYP2C19 inhibitor	CYP2C9 inhibitor	CYP2D6 inhibitor	CYP3A4 inhibitor
1	No	Yes	Yes	Yes	No	No	No
2	No	No	Yes	No	No	No	No
3	No	No	No	No	No	No	No
6	No	Yes	Yes	Yes	No	No	No

*The red color indicates that the ligand does not meet the criteria of the corresponding parameter

Table 9
The excretion profile evaluation results of the hits.

Ligands	Total Clearance (ml/ mnt/kg)	OCT2 Substrate
1	0.142	No
2	0.094	No
3	0.263	No
6	0.130	No

which serine is one of the catalytic triad next to histidine and aspartate, located at the catalytic domain [44]. In the ligand **6**′s pose, GLU166 could hold the O-amide to let the water attacks the amide bond leading to hydrolysis. This could be the mode of action on how ligand **6** distracts the interaction of M^{pro} with its substrate, thus it acts as a competitive inhibitor. However, an experimental kinetic study should be performed to confirm this.

In the real experiment (*in vitro*), a drug candidate should be confirmed their true-positive activity by adding detergent (0.01–0.05% Tween-20) [45]. This detergent is purposed to avoid aggregate interference, that sometime/ frequently happen during *in vitro* enzymatic assay, which could lead to the false-positive result. This positive result could not be due to the enzyme-tested compound chemical interaction, but rather to compound's aggregation, that buries the enzyme's binding pocket leading to a false-positive result. A number of compounds have been identified to be a potential PAINS compounds such as toxoflavine, isothiazolone, curcumin, hydroxyphenyl hydrazone, ene-rhodanine, and phenol-sulphonamide [25]. This work surely increases the time and cost of experiment because the tested samples could be thousands or even more. Therefore, the development of PAINS filter using online tool is a great innovation to reduce time and cost of research.

The efficiency of hit to be developed as drug candidates are measured by calculating the efficiency in each parameter, employing drug-like structure, toxicity, absorption, distribution, metabolism and excretion. These are calculated by dividing the number of permitted criteria over the total number of criteria, and then multiplied by 100 to obtain an efficiency percentage. For example, the toxicity in Table 5, ligand **1** showed seven of 10 criteria, which passed the mutagenicity and toxicity requirement, therefore, it is calculated as 70, etc. The efficiency percentages are presented in Table 10. In the drug-like structure properties, all hits meet 100% of the criteria including MW, log P, HBD, HBA, rotatable bonds and surface area. The mutagenicity and toxicity profiles show 60–70% agreement of all hits with the requirements, whereas the percentages are quite high to meet the absorption criteria. As such, the distribution criteria are 75–100% passed by all hits. Ligand **1** and **6** are taken into account, as these hits could be 43% potentially interfering the CYP activities in drug metabolisms. Interestingly, all hits are fully meeting the excretion criteria. The average of all properties is drawn resulting the efficiency of all hits by 84 to 88% as drug candidates.

This study is limited by no dynamics behaviour investigated and performed to confirm the stability of the ligand while interacting with the M^{pro}. The post-MD binding energy should be calculated using methods such as Molecular Mechanics Poisson-Boltzmann Surface Area (MMPBSA) or Molecular Mechanics Generalised Born Surface Area (MMGBSA), which is closer to the real condition than the docking energy calculation only. However, due to our limitation, we plan to perform this MD after synthesizing and experimentally testing the potential compound from this study.

Conclusion

A series of 2-phenoxyacetamide derivatives have been designed as SARS-CoV-2 M^{pro} inhibitor by approaching a deal of a feasible synthesis dan a selective pharmacophore. The initial *in silico* screening selects four hit compounds with four highest fit score with the common pharmacophore features being HBA and H. These hits were further studied for their binding affinity as well as chemical interactions with the M^{pro} binding pocket. The docking result shows an agreement with the pharmacophore study, in which ligand with $COCH_3$ at *para* position toward the arylamide phenyl ring, possessing the strongest binding with the M^{pro} as well as with the pharmacophore of such enzyme's inhibitor. The PAINS filter suggests, that all hits do not have a potential aggregation during *in vitro* assay. The potency as a drug candidate was further evaluated based on drug-like structure, mutagenic potency and toxicity, and ADMET showing that all hits considerably meet the criteria as a drug candidate, by showing 84–88% efficiency. In conclusion, 2-phenoxyacetamide derivatives are potential to be processed as lead compound for SARS-CoV-2 M^{pro}.

Data availability

The data soft files are available in this below link, https://drive.google.com/drive/folders/1m6oTtl_kXfyjz4IGt3rypNXO_o8rxl5Y?usp=sharing.

Funding

This work was financially supported by Internal Grant with the scheme of Doctoral-Master Research of Lembaga Penelitian dan Pengabdian Masyarakat (LPPM), Sanata Dharma University with the grant no. 013/Penel./LPPM-USD/II/2021. Further research funding was supported by Indonesia Toray Science Foundation (ITSF) under Science and Technology Research Grant (STRG) 2020.

Table 10
The efficiency percentage of the hits in drug-like structure, toxicity, absorption, distribution, metabolism and excretion.

Ligand	Drug-like Structure	Toxicity	Absorption	Distribution	Metabolism	Excretion	Mean
1	100	70	100	100	57	100	88
2	100	60	86	75	86	100	85
3	100	60	71	75	100	100	84
6	100	70	100	100	57	100	88

CRediT authorship contribution statement

Pandu Hariyono: Writing, Investigation. **Rini Dwiastuti:** Writing – review & editing. **Muhammad Yusuf:** Writing – review & editing. **Nurul H. Salin:** Writing – review & editing. **Maywan Hariono:** Conceptualization, Writing – review & editing.

Declaration of Competing Interest

The authors declare that they have no known competing financial interests or personal relationships that could have appeared to influence the work reported in this paper.

Acknowledgement

We greatly acknowledge the Scripps Research Institute, PubChem, ACD/Labs, and Dassault Systems for freely providing AutoDock, 3D structure, ACD/ Chemsketch, and Biovia Discovery Studio softwares.

References

[1] https://covid19.who.int/ (accessed September 16, 2021).
[2] C.H. Liu, C.H. Lu, S.H. Wong, L.T. Lin, Update on antiviral strategies against COVID-19: Unmet needs and prospects, Front. Immunol. 11 (2020).
[3] R. Agarwal, G. Gopinath, A proposal to end the COVID-19 pandemic. Staff Discussion, Notes. 2021 (004) (2021) 1, https://doi.org/10.5089/9781513577609.006.
[4] M.S. Hossain, I. Hami, M.S.S. Sawrav, M.F. Rabbi, O. Saha, N.M. Bahadur, M. M. Rahaman, Drug repurposing for prevention and treatment of COVID-19: a clinical landscape, Discoveries. 8 (4) (2020 Oct) e121, https://doi.org/10.15190/d.2020.18.
[5] Lansdowne LE. Target identification & validation in drug discovery.
[6] T.M. Bakheet, A.J. Doig, Properties and identification of human protein drug targets, Bioinformatics 25 (4) (2009 Feb 15) 451–457.
[7] Y. Hartini, B. Saputra, B. Wahono, Z. Auw, F. Indayani, L. Adelya, G. Namba, M. Hariono, Biflavonoid as potential 3-chymotrypsin-like protease (Mpro) inhibitor of SARS-Coronavirus, Res. Chem. 1 (3) (2021), 100087.
[8] P. Hariyono, C. Patramurti, D.S. Candrasari, M. Hariono, An integrated virtual screening of compounds from Carica papaya leaves against multiple protein targets of SARS-Coronavirus-2, Res. Chem. 3 (2021) 100113, https://doi.org/10.1016/j.rechem.2021.100113.
[9] M.S. Zubair, S. Maulana, A. Widodo, R. Pitopang, M. Arba, M. Hariono, GC-MS, LC-MS/MS, docking and molecular dynamics approaches to identify potential SARS-CoV-2 3-chymotrypsin-like protease inhibitors from zingiber officinale roscoe, Molecules 26 (17) (2021) 5230.
[10] A. Citarella, A. Scala, A. Piperno, N. Micale, SARS-CoV-2 Mpro: A Potential Target for Peptidomimetics and Small-Molecule Inhibitors, Biomolecules. 11 (4) (2021) 607.
[11] Stoermer M. Homology Models of Coronavirus 2019-nCoV Mpro Protease. ChemRxiv, 2020. Preprint. https://doi. org/10.26434/chemrxiv.;11637294:v3.
[12] Z. Jin, X. Du, Y. Xu, Y. Deng, M. Liu, Y. Zhao, B. Zhang, X. Li, L. Zhang, C. Peng, Y. Duan, J. Yu, L. Wang, K. Yang, F. Liu, R. Jiang, X. Yang, T. You, X. Liu, X. Yang, F. Bai, H. Liu, X. Liu, L.W. Guddat, W. Xu, G. Xiao, C. Qin, Z. Shi, H. Jiang, Z. Rao, H. Yang, Structure of M pro from SARS-CoV-2 and discovery of its inhibitors, Nature 582 (7811) (2020) 289–293.
[13] H.M. Mengist, T. Dilnessa, T. Jin, Structural basis of potential inhibitors targeting SARS-CoV-2 Mpro. Frontiers, Chemistry. 9 (2021).
[14] B.J. Bruno, G.D. Miller, C.S. Lim, Basics and recent advances in peptide and protein drug delivery, Therapeutic delivery. 4 (11) (2013) 1443–1467.
[15] B.K. Yap, C.-Y. Lee, S.B. Choi, E.E. Kamarulzaman, M. Hariono, H.A. Wahab, Silico Identification of Novel Inhibitors, Encyclopedia of Bioinformatics and Computational Biology, Academic Press, 2019, pp. 761–779.
[16] P. Magro, I. Zanella, M. Pescarolo, F. Castelli, E. Quiros-Roldan, Lopinavir/ritonavir: Repurposing an old drug for HIV infection in COVID-19 treatment, Biomed. J. 44 (1) (2021) 43–53.
[17] P. Rani, D. Pal, R. Hegde, S. Hashim, Synthesis, characterization and pharmacological evaluation of substituted phenoxy acetamide derivatives, Hemijska industrija. 69 (4) (2015) 405–415.
[18] M. Hariono, H.A. Wahab, M.L. Tan, M.M. Rosli, I.A. Razak, 9-Benzyl-6-benzylsulfanyl-9H-purin-2-amine, Acta Crystallogr. Sect. E: Struct. Rep. Online 70 (3) (2014) o288.
[19] F.D.O. Riswanto, M.S.A. Rawa, V. Murugaiyah, N.H. Salin, E.P. Istyastono, M. Hariono, H.A. Wahab, Anti-cholinesterase activity of chalcone derivatives: Synthesis, in vitro assay and molecular docking study, Med. Chem. 17 (5) (2021) 442–452.
[20] H.-X. Su, S. Yao, W.-F. Zhao, M.-J. Li, J. Liu, W.-J. Shang, H. Xie, C.-Q. Ke, H.-C. Hu, M.-n. Gao, K.-Q. Yu, H. Liu, J.-S. Shen, W. Tang, L.-k. Zhang, G.-f. Xiao, L. i. Ni, D.-W. Wang, J.-P. Zuo, H.-L. Jiang, F. Bai, Y. Wu, Y. Ye, Y.-C. Xu, Anti-SARS-CoV-2 activities in vitro of Shuanghuanglian preparations and bioactive ingredients, Acta Pharmacol. Sin. 41 (9) (2020) 1167–1177.
[21] M. Hariono, P. Hariyono, R. Dwiastuti, W. Setyani, M. Yusuf, N. Salin, H. Wahab, Potential SARS-CoV-2 Mpro inhibitors from chromene, flavonoid and hydroxamic acid compound based on fret assay, docking and pharmacophore studies, Res. Chem. 3 (2021) 100195.
[22] G.M. Morris, R. Huey, W. Lindstrom, M.F. Sanner, R.K. Belew, D.S. Goodsell, A. J. Olson, AutoDock4 and AutoDockTools4: Automated docking with selective receptor flexibility, J. Comput. Chem. 30 (16) (2009) 2785–2791.
[23] J.B. Baell, G.A. Holloway, New substructure filters for removal of pan assay interference compounds (PAINS) from screening libraries and for their exclusion in bioassays, J. Med. Chem. 53 (7) (2010) 2719–2740.
[24] D.E.V. Pires, T.L. Blundell, D.B. Ascher, pkCSM: predicting small-molecule pharmacokinetic and toxicity properties using graph-based signatures, J. Med. Chem. 58 (9) (2015) 4066–4072.
[25] J. Baell, M.A. Walters, Chemistry: Chemical con artists foil drug discovery, Nature News. 513 (7519) (2014) 481–483.
[26] C.A. Lipinski, Drug-like properties and the causes of poor solubility and poor permeability, J. Pharmacol. Toxicol. Methods 44 (1) (2000) 235–249.
[27] Armstrong JD, Hubbard RE, Farrell T, Maiguashca B (2006) Structure-based Drug Discovery: An Overview.
[28] E. Huerta, N. Grey, Cancer Control Opportunities in Low- and Middle-income Countries, CA Cancer J. Clin. 57 (2) (2007) 72–74.
[29] D.L. McCormick, Preclinical Evaluation of Carcinogenicity Using Standard-Bred and Genetically Engineered Rodent Models, Elsevier Inc, Second Edi, 2017.
[30] D. Gadaleta, K. Vuković, C. Toma, G.J. Lavado, A.L. Karmaus, K. Mansouri, N. C. Kleinstreuer, E. Benfenati, A. Roncaglioni, SAR and QSAR modeling of a large collection of LD 50 rat acute oral toxicity data, J. Cheminf. 11 (1) (2019 Dec) 1–6.
[31] Barlow S, Chesson A, Collins JD, Flynn A, Hardy A, Jany KD, Knaap A, Kuiper H, Larsen JC, Lovell D, Le Neindre P. Use of the benchmark dose approach in risk assessment Guidance of the Scientific Committee. EFSA JOURNAL. 2009 Jun 1;7 (6).
[32] T.L. Sorell, Approaches to the development of human health toxicity values for active pharmaceutical ingredients in the environment, AAPS J. 18 (1) (2016) 92–101.
[33] I.D. Angelis, L. Turco, Caco-2 cells as a model for intestinal absorption, Curr. Prot. Toxicol. 47 (1) (2011) 20–26.
[34] J.H. Lin, M. Yamazaki, Role of P-glycoprotein in pharmacokinetics, Clin. Pharmacokinet. 42 (1) (2003) 59–98.
[35] P. Ballabh, A. Braun, M. Nedergaard, The blood–brain barrier: an overview: structure, regulation, and clinical implications, Neurobiol. Dis. 16 (1) (2004) 1–13.
[36] M.T. Kinirons, M.S. O'Mahony, Drug metabolism and ageing, Br. J. Clin. Pharmacol. 57 (5) (2004) 540–544.
[37] S.E. Rosenbaum (Ed.), Basic Pharmacokinetics And Pharmacodynamics: An Integrated Textbook And Computer Simulations, John Wiley & Sons, 2016 Dec 27.
[38] H.J. Burt, S. Neuhoff, L. Almond, L. Gaohua, M.D. Harwood, M. Jamei, A. Rostami-Hodjegan, G.T. Tucker, K. Rowland-Yeo, Metformin and cimetidine: Physiologically based pharmacokinetic modelling to investigate transporter mediated drug–drug interactions, Eur. J. Pharm. Sci. 10 (88) (2016 Jun) 70–82.
[39] P.L. Toutain, A. Bousquet-melou, Plasma clearance, J. Vet. Pharmacol. Ther. 27 (6) (2004) 415–425.
[40] P.K. Deb, O. Al-Attraqchi, A.Y. Jaber, B. Amarji, R.K. Tekade, Physicochemical Aspects To Be Considered In Pharmaceutical Product Development, in: Dosage Form Design Considerations, Elsevier, 2018, pp. 57–83.
[41] W. Shen, S. Yu, J. Zhang, W. Jia, Q. Zhu, Synthesis and biological evaluation of 2-phenoxyacetamide analogues, a novel class of potent and selective monoamine oxidase inhibitors, Molecules 19 (11) (2014) 18620–18631.
[42] J.D. Williams, M.C. Torhan, V.R. Neelagiri, C. Brown, N.O. Bowlin, M. Di, C. T. McCarthy, D. Aiello, N.P. Peet, T.L. Bowlin, D.T. Moir, Synthesis and structure–activity relationships of novel phenoxyacetamide inhibitors of the Pseudomonas aeruginosa type III secretion system (T3SS), Bioorg. Med. Chem. 23 (5) (2015) 1027–1043.
[43] T. Sutradhar, A. Misra, Role of electron-donating and electron-withdrawing groups in tuning the optoelectronic properties of difluoroboron-napthyridine analogues, J. Phys. Chem. A. 122 (16) (2018) 4111–4120.
[44] L. Hedstrom, Serine protease mechanism and specificity, Chem. Rev. 102 (12) (2002) 4501–4524.
[45] B.Y. Feng, B.K. Shoichet, A detergent-based assay for the detection of promiscuous inhibitors, Nat. Protoc. 1 (2) (2006) 550–553.